arXiv:1304.2804v1 [cond-mat.mes-hall] 9 Apr 2013

Possibility for exciton Bose-Einstein condensation in carbon nanotubes

I. V. Bondarev and A. V. Meliksetyan
Department of Math & Physics, North Carolina Central University, Durham, NC 27707, USA

We demonstrate the possibility of exciton Bose-Einstein condensation in individual small-diameter ($\sim 1-2$ nm) semiconducting carbon nanotubes. The effect occurs under the exciton-interband-plasmon coupling controlled by an external electrostatic field applied perpendicular to the nanotube axis. It requires fields $\sim$1 V/nm and temperatures below 100 K that are experimentally accessible.

Carbon nanotubes (CNs), graphene sheets rolled-up into cylinders of one to a few nanometers in diameter and up to hundreds of microns in length, have been successfully integrated into miniaturized electronic, electromechanical, chemical devices, scanning probes, and into nanocomposite materials [1, 2]. Over the past few years, optical nanomaterials research has uncovered intriguing optical attributes of their physical properties [3], as well, lending themselves to a variety of optoelectronic device applications [3–14]. The great breadth and depth of optical phenomena in CNs is exemplified by experimental and theoretical reports on how their optical properties are affected by defects [15, 16], exciton-phonon interactions [17], biexciton formation [18, 19], exciton-plasmon coupling [20], external magnetic [21] and electric fields [20, 22]. Recent studies have also looked at thermal rectification [23], microwave-frequency signal rectification [24] and non-linear optical response of individual CNs [25]. Several recent efforts reported on semiconducting CNs used for the generation, detection and harvesting of light [6–13], and as single photon sources for quantum computing, communication, or cryptography [26–28].

Undoped semiconducting single-wall CNs are direct band-gap semiconductors and feature very large exciton binding energies (hundreds of meV) [4, 5], which one can vary in controllable ways to modify their underlying optical properties. This offers new functionality and creates a very strong potential for future tunable optoelectronic device applications with individual CNs. Excitons in CNs can be affected by either electrostatic doping [9, 29] or by the quantum confined Stark effect (QCSE) [12, 20] (an external electrostatic field applied perpendicular to the CN axis; the effect is used recently to tune the bandgap of bilayer graphene [30]). In both cases, exciton properties are mediated by collective plasmon excitations. QCSE, in particular, allows one to control exciton-interband-plasmon coupling in individual undoped CNs and their (linear [12, 13, 20] and nonlinear [19, 31]) optical absorption [32]. By varying the exciton-plasmon coupling strength with the QCSE one controls both the radiative exciton emission and non-radiative exciton-to-plasmon energy transfer. This latter phenomenon is similar to the SPASER effect (Surface Plasmon Amplification by Stimulated Emission of Radiation) reported earlier for hybrid metal-semiconductor-dielectric nanostructures [33]. It takes place in *individual* small-diameter CNs though, resulting in new strongly coupled hybridized excitations — exciton-plasmons — and associated high-intensity coherent oscillating fields concentrated locally along the CN surface [12, 13]. These near-fields can be used in a variety of new optoelectronic applications, including near-field nonlinear-optical probing and sensing, optical switching, enhanced electromagnetic absorption, and materials nanoscale modification.

Apart from applications, carbon nanotubes offer an ideal testing ground to study the fundamentals of condensed matter physics in one dimension (1D). Here, we discuss possibilities for the 1D Bose-Einstein condensation (BEC) phenomenon that originates from the strong coupling of excitons and inter-band (same-band) plasmons enabled by using the QCSE. Exciton-plasmons thus created in an individual nanotube are strongly correlated collective Bose excitations and, therefore, could likely be condensed under appropriate external conditions — in spite of the well-known statements of the BEC impossibility in ideal 1D/2D systems [34] and experimental evidence for no exciton BEC effect in CNs [35]. Possibilities for achieving BEC in 1D and 2D systems are theoretically demonstrated in the presence of an extra confinement potential [36]. We show that the strongly correlated exciton-plasmon system in a CN presents such a special case. We find the critical BEC temperature, as well as the condensate fraction and its exciton contribution as functions of temperature and electrostatic field applied. We discuss how the effect can be observed experimentally.

Figure 1 shows our calculations of the dynamical axial conductivities for a few representative semiconducting CNs, (13,0), (16,0), (20,0) and (26,0), of increasing diameters $\sim 1-2$ nm ($R_{CN}=0.51, 0.63, 0.78$ and 1.02 nm, respectively). In small-diameter CNs, excitons are excited by the external electromagnetic (EM) radiation polarized along the CN axis [37]. So, only the axial conductivity σ_{zz} matters while the azimuthal one $\sigma_{\varphi\varphi}$ can be neglected being strongly suppressed due to the transverse depolarization effect [we use cylindrical coordinates, Fig. 2 (a), with the z-axis being the CN axis]. To calculate σ_{zz}, we used the $(\mathbf{k}\cdot\mathbf{p})$-method of Ref. [37] with the exciton relaxation time 100 fs for all four CNs (consistent with previous estimates [17, 22]). Many-particle Coulomb correlations are included by solving the Bethe-Salpeter equation in the momentum space within the screened Hartree-Fock approximation as described in Ref. [37]. Real conductivities consist of series of peaks $(E_{11}, E_{22}, ...)$ representing the 1st, 2nd, etc., excitons. Imaginary conductivities are linked with the real ones by the Kramers-Kronig relation. That is why the functions

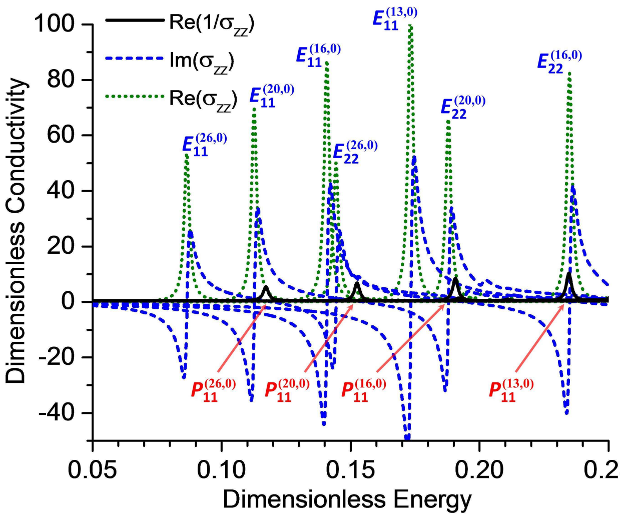

FIG. 1: (Color online) Calculated energy dependence of the dimensionless (normalized by $e^2/2\pi\hbar$) axial surface conductivity σ_{zz} for the four zigzag nanotubes, (13,0), (16,0), (20,0) and (26,0), of increasing diameters. Peaks of $\mathrm{Re}\,\sigma_{zz}$ represent excitons (E_{11}, E_{22}); peaks of $\mathrm{Re}(1/\sigma_{zz})$ represent inter-band plasmons (P_{11}, P_{22}). Dimensionless energy is defined as $[Energy]/2\gamma_0$, where $\gamma_0 = 2.7$ eV is the C-C overlap integral.

$\mathrm{Re}(1/\sigma_{zz}) = \mathrm{Re}(\sigma_{zz})/\{[\mathrm{Re}(\sigma_{zz})]^2 + [\mathrm{Im}(\sigma_{zz})]^2\}$ show the resonances $P_{11}, P_{22}, \ldots$ right next to $E_{11}, E_{22}, \ldots$. These are the inter-band plasmon resonances (first studied experimentally in Ref. [38]) as $\mathrm{Re}(1/\sigma_{zz})$ is directly related to $\mathrm{Im}(1/\epsilon_{zz})$, the electron-energy-loss spectroscopy response (ϵ_{zz} is the longitudinal dielectric function) representative of plasmon excitations in the system [38].

Perpendicular electrostatic field [Fig. 2 (a)] mixes exciton and plasmon resonances, to result in two branches of new hybridized quasi-particle states, exciton-plasmons, with the energies (dimensionless variables, see Ref. [20])

$$x_{1,2} = \sqrt{\frac{\varepsilon_f^2 + x_p^2}{2} \pm \frac{1}{2}\sqrt{(\varepsilon_f^2 - x_p^2)^2 + (2X_f)^2 \varepsilon_f x_p}}\,, \quad (1)$$

where $\varepsilon_f = E_f(\mathbf{k})/2\gamma_0$ and $x_p = E_p/2\gamma_0$ are the energies of the f-internal-state exciton and inter-band plasmon of the same band, respectively, with $\gamma_0 = 2.7$ eV being the C-C overlap integral, $X_f = [2\Delta x_p \bar{\Gamma}_0^f(x_p)\rho(x_p)]^{1/2}$ is the exciton-plasmon Rabi-splitting taken at energy $x = x_p$, where $\bar{\Gamma}_0^f$ is the exciton spontaneous decay (radiative recombination) rate and $\rho(x) \approx \rho(x_p)\Delta x_p^2/[(x-x_p)^2 + \Delta x_p^2]$ is the Lorentzian approximated (of half-width-at-half-maximum Δx_p) density-of-states (DOS) representing the non-radiative coupling of excitons to plasmons. Exciton quasi-momentum $\mathbf{k} = \{k_\varphi, k_z\}$ is a two-component vector with quantized k_φ and continuous k_z to represent the longitudinal motion of the exciton center-of-mass, so that $E_f(\mathbf{k}) = E_{exc}^{(f)}(k_\varphi) + \hbar^2 k_z^2/2M_{ex}(k_\varphi)$ with the first term $E_{exc}^{(f)}(k_\varphi) = E_g(k_\varphi) + E_b^{(f)}(k_\varphi)$ being the exciton excitation energy $\{E_g$ is the band gap, $E_b^{(f)}$ is the (negative) binding energy; these, as well as x_p, are affected by the QCSE, see Ref.[20]$\}$ and the second term being the kinetic energy of the translational longitudinal motion of the exciton with the effective mass $M_{ex} = m_e + m_h$, where $m_{e,h}$ are the electron (hole) effective masses.

Figure 2 (b) shows an example of the two exciton-plasmon branches given by Eq. (1) as functions of the perpendicular electrostatic field F [geometry shown in Fig. 2 (a)] and longitudinal momentum for the lowest bright ground-internal-state exciton (in which case we omit the f-subscript in what follows) coupled to the nearest inter-band plasmon in the (20,0) nanotube [$E_{11}^{(20,0)}$ and $P_{11}^{(20,0)}$ in Fig. 1]. The origin of energy is taken to be $x_2(F, k_z = 0)$. In non-zero field $F_c \approx 2$ V/nm, where the strong exciton-plasmon coupling occurs, the upper branch x_1 has the global minimum at zero momentum, $k_z^c = k_z(F_c) = 0$, separated from the lower branch by the Rabi-splitting $X(F_c, 0)$. Hence, at equilibrium, if the temperature T is such that $k_B T/2\gamma_0 > X(F_c, 0)$, strongly coupled upper-branch exciton-plasmons will be distributed around this minimum in the momentum space. Lowering T to get $k_B T/2\gamma_0 < X(F_c, 0)$ will push them all down to occupy the lowest possible energy state, the $k_z = 0$ state, which is nothing but the exciton-plasmon BEC effect. This effect does not depend on the density of particles though, as opposed to the BEC of

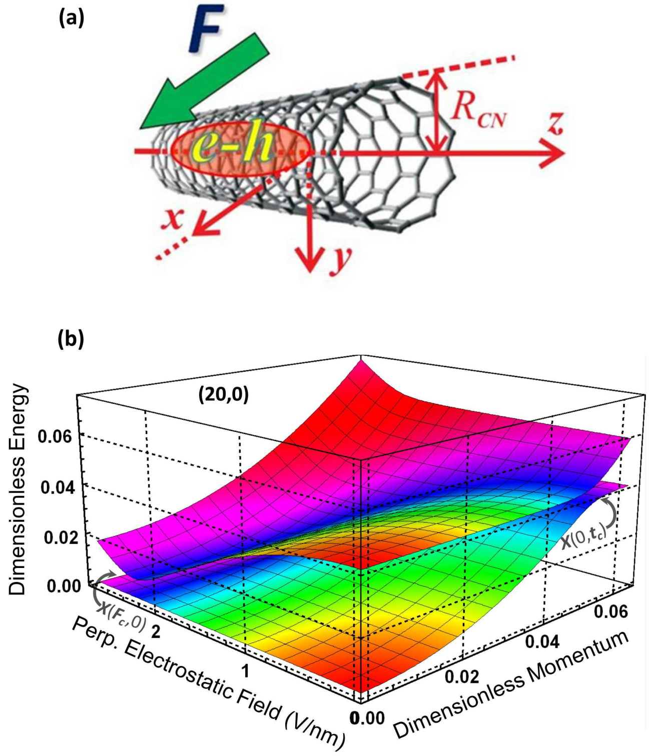

FIG. 2: (Color online) (a) The geometry of the problem. (b) Exciton-plasmon dispersion as a function of the perpendicular electrostatic field and longitudinal momentum for the lowest bright exciton coupled to the nearest inter-band plasmon in the (20,0) nanotube ($E_{11}^{(20,0)}$ and $P_{11}^{(20,0)}$ in Fig. 1). See text for dimensionless momentum.

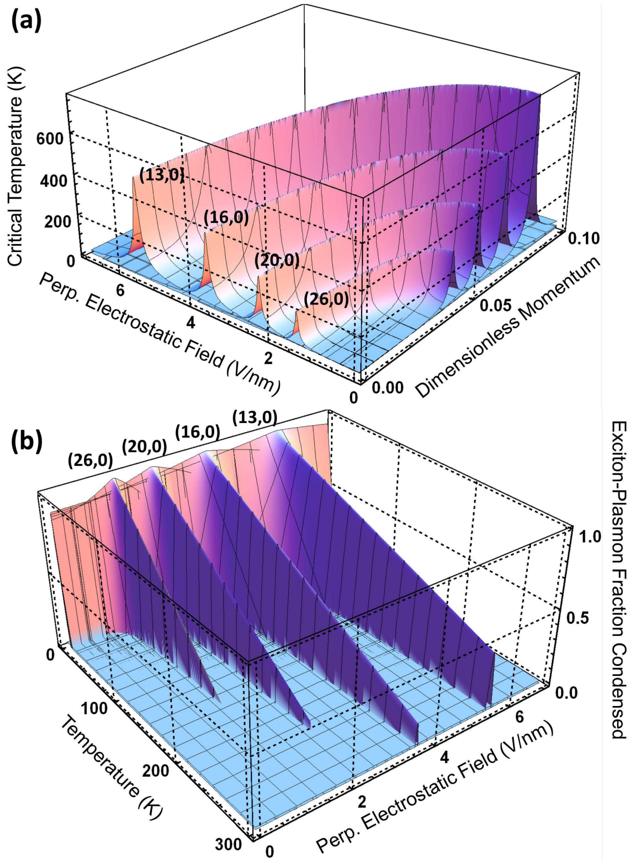

FIG. 3: (Color online) Critical temperatures (a) as functions of the perpendicular electrostatic field applied and longitudinal momentum, and mean upper-branch BEC population fractions (b) as given by Eq. (2), for the four CNs under consideration. See text for dimensionless momentum.

non-interacting massive bosons [34, 39]. Therefore, it is hardly sensitive to the interaction, if any, between exciton-plasmons. Rather, this BEC effect is the characteristic feature of the quasi-particle energy spectrum of the coupled exciton-plasmon excitations in our system.

It is not difficult to derive the BEC fraction as a function of T and F. At $k_z\sim k_z^c$, wherein $\varepsilon_f\sim x_p$, Eq. (1) expands into $x_1(F,s,t)\approx X_f[s,t_c(F)]+\alpha(s)\,t^2/2$, with the energy counted from $x_2(F,t\!=\!0)$, $t\!=\!k_z/\tilde{k}_z$ being the dimensionless longitudinal quasi-momentum ($|t|\leq 1$) and $\alpha=\hbar^2\tilde{k}_z^2/2M_{ex}(s)$. The first Brillouin zone of the CN of (m,n) type ($n\leq m$) is taken to be consisting of m parallel lines, as per quantized $k_\varphi=k_\varphi(s)=s/R_{CN}$ with $s=1,2,...,m$ and $R_{CN}=(\sqrt{3}\,b/2\pi)\sqrt{m^2+mn+n^2}$, each of length $2\tilde{k}_z=2B/k_\varphi(m)$, where $2B=2(4\pi^2/3\sqrt{3}\,b^2)$ is the rectangular area of the reciprocal space covered by the lines, $b=1.42$ Å is the C-C interatomic distance [12]. To obtain the mean upper-branch BEC population fraction $\langle n_{10}\rangle$, we use this x_1 and employ the conventional technique (e.g., Refs. [34, 39]) to perform the summation over $\mathbf{k}$ in the first Brillouin zone. For the ground-internal-state exciton, assuming $M_{ex}(s)\approx M_{ex}$ and $X_f[s,t_c(F)]\approx X_f[t_c(F)]=X(F)$, this results in

$$\langle n_{10}\rangle(T\!<\!T_c,F)\approx 1-T/T_c(F), \qquad (2)$$

where $T_c(F)=2\gamma_0X(F)/k_B$ is the critical temperature with $X(F)=\{2\Delta x_p\bar{\Gamma}_0[\varepsilon(F,t\!=\!0)]\rho[\varepsilon(F,t\!=\!0)]\}^{1/2}$ standing for the exciton-plasmon Rabi-splitting at the (excitation) energy of the zero-momentum ground-state exciton. This latter one controls the convergence of the result.

Figure 3 (a) shows calculated T_c as functions of F and t (to better understand the general behavior), for the lowest bright ground-internal-state excitons coupled to the nearest inter-band plasmons in the four CNs under consideration. The functions $T_c(F,t)$ are resonance shaped of widths $\sim 2\Delta x_p$, peaked at $\varepsilon(F,t)\approx x_p(F)$. As F increases, the peak positions shift down to $t\sim 0$, yielding field dependent, resonance shaped $T_c(F)$, same as $X(F)$, peaked at $F_c\sim 1-6$ V/nm with maximum $T_c\sim 150-500$ K and greater F_c and T_c for smaller diameter CNs. Figure 3 (b) presents $\langle n_{10}\rangle$ as given by Eq. (2) for the same case. The quantities $\langle n_{10}\rangle$ reflect the behavior of $T_c(F)$, showing finite BEC fractions throughout the finite ranges of F centered about F_c, expanding in F as T decreases.

Following the general theory of the exciton-plasmon interactions in individual CNs [20], one can now calculate the exciton participation rate in the exciton-plasmon BEC population fraction (2). This is represented by the absolute value squared of the ratio of the exciton mixing coefficient to the plasmon mixing coefficient of the upper exciton-plasmon branch. Using the mixing coefficients of Ref.[20] yields thus defined exciton fraction condensed as a function of dimensionless energy x, T and F as follows

$$\langle n_{10}\rangle_{E/P}(x,T,F)\approx\frac{\pi\Delta x_p(x-x_1)^2(1+x_1/\varepsilon)^2}{X^2(F)}\langle n_{10}\rangle \quad (3)$$

with energies to be counted from $x_2(F,t\!=\!0)$. Comparing this with Fig. 2 (b), we see that at $x=0$ corresponding to the first ground-state-exciton excitation energy and $F=F_c$ [resonance condition yielding $x_1=X(F_c)$ and $\varepsilon=X(F_c)/2$], Eq. (3) becomes $9\pi\Delta x_p\langle n_{10}\rangle\ll 1$, meaning that the exciton-plasmon BEC is dominated by plasmons. This is consistent with the coherent plasmon generation effect by excitons reported lately [12, 13]. A slight detuning from F_c increases x_1 and dramatically decreases $X(F)$ [Fig. 3 (a)], bringing about bursts of $\langle n_{10}\rangle_{E/P}\gg 1$,

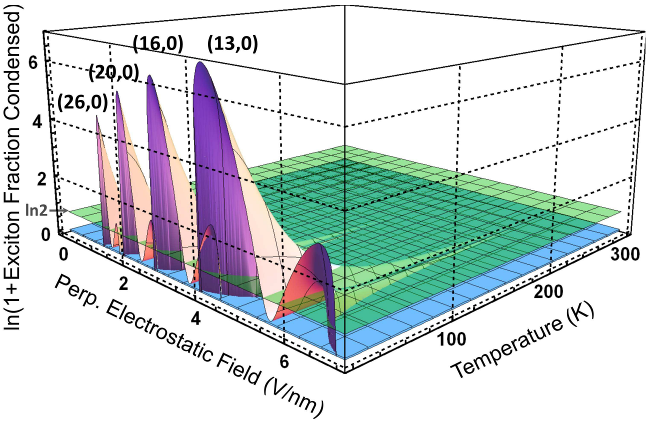

FIG. 4: (Color online) Function $\ln[1+\langle n_{10}\rangle_{E/P}(0,T,F)]$ calculated using Eqs. (2) and (3) for the CNs under consideration.

making the exciton-plasmon BEC dominated by excitons.

The exciton BEC effect is shown in Fig. 4 for the CNs under consideration. It occurs at $F \gtrsim 1$ V/nm and $T \lesssim 100$ K that are experimentally accessible [30]. The effect is stronger and covers broader range of F and T in smaller diameter CNs. Off-resonance coupling to interband plasmons, which are just *standing* charge density waves, slows excitons down by pushing them into periodic effective potential "traps", thus increasing zero-translational-momentum exciton state population. This is consistent with earlier studies where the 1D/2D BEC phenomenon, otherwise prohibited [34], is shown to occur in the presence of an extra confinement potential [36].

The effect of the exciton BEC presented here will manifest itself as highly coherent, longitudinally polarized, far-field exciton emission appearing at temperatures below 100 K as one smoothly increases the perpendicular field strength. Narrow BEC emission peak will be blue shifted by the Rabi-splitting energy from the first exciton excitation energy which the CN should be pumped at by an external laser source. The phenomenon can be investigated in experiments similar to those used for exciton-polariton BEC studies in semiconductor microcavities [40].

Discussions with J. Anders of UCL, UK, are acknowledged. I.V.B. is supported by DOE (DESC0007117); A.V.M. is funded by ARO (W911NF-11-1-0189).

[1] M.Dresselhaus, G.Dresselhaus, and Ph.Avouris (eds.), Carbon Nanotubes: Synthesis, Structure, Properties, and Applications (Springer-Verlag, Berlin, 2001).

[2] R.H.Baughman, A.A.Zakhidov, W.A.DeHeer, Science **297**, 787 (2002).

[3] T.Hertel and I.V.Bondarev (eds.), Photophysics of Carbon Nanotubes and Nanotube Composites (Special issue), Chem. Phys. **413**, 1 (2013).

[4] M.S.Dresselhaus, G.Dresselhaus, R.Saito, and A.Jorio, Annu. Rev. Phys. Chem. **58**, 719 (2007).

[5] Ph.Avouris, M.Freitag, and V.Perebeinos, Nature Photon. **2**, 341 (2008).

[6] F.Vietmeyer, B.Seger, and P.V.Kamat, Advanced Materials **19**, 2935 (2007).

[7] N.M.Gabor, Z.Zhong, K.Bosnick, J.Park, and P.L.McEuen, Science **325**, 1367 (2009).

[8] T.Hertel, Nature Photon. **4**, 77 (2010).

[9] T.Mueller, M.Kinoshita, M.Steiner, V.Perebeinos, A.A.Bol, D.B.Farmer, and Ph.Avouris, Nature Nanotech. **5**, 27 (2010).

[10] X.Dang, H.Yi, M.-H.Ham, J.Qi, D.S.Yun, R.Ladewski, M.S.Strano, P.T.Hammond, and A.M.Belcher, Nature Nanotechn. **6**, 377 (2011).

[11] E.Malic, C.Weber, M.Richter, V.Atalla, T.Klamroth, P.Saalfrank, S.Reich, and A.Knorr, Phys. Rev. Lett. **106**, 097401 (2011).

[12] I.V.Bondarev, Phys. Rev. B **85**, 035448 (2012).

[13] I.V.Bondarev and T.Antonijevic, Phys. Stat. Sol. C **9**, 1259 (2012).

[14] S.Nanot, E.H.Haroz, J.-H.Kim, R.H.Hauge, and J.Kono, Advanced Materials **24**, 4977 (2012).

[15] A.Hagen, M.Steiner, M.B.Raschke, C.Lienau, T.Hertel, H.Qian, A.J.Meixner, and A.Hartschuh, Phys. Rev. Lett. **95**, 197401 (2005).

[16] B.O.Tayo and S.V.Rotkin, Phys. Rev. B 86, 125431 (2012).

[17] S.Piscanec, M.Lazzeri, J.Robertson, A.Ferrari, and F.Mauri, Phys. Rev. B **75**, 035427 (2007).

[18] T.G.Pedersen, K.Pedersen, H.D.Cornean, and P.Duclos, NanoLett. **5**, 291 (2005).

[19] I.V.Bondarev, Phys. Rev. B **83**, 153409 (2011).

[20] I.V.Bondarev, L.M.Woods, and K.Tatur, Phys. Rev. B **80**, 085407 (2009); Opt. Commun. **282**, 661 (2009).

[21] A.Srivastava, H.Htoon, V.I.Klimov, and J.Kono, Phys. Rev. Lett. **101**, 087402 (2008).

[22] V.Perebeinos and Ph.Avouris, NanoLett. 7, 609 (2007).

[23] C.W.Chang, D.Okawa, A.Majumdar, and A.Zettl, Science **314**, 1121 (2006).

[24] E.Cobas and M.Fuhrer, Appl. Phys. Lett. **93**, 043120 (2008).

[25] P.Myllyperkio, O.Herranen, J.Rintala, H.Jiang, P.R.Mudimela, Z.Zhu, A.G.Nasibulin, A.Johansson, E.I.Kauppinen, M.Ahlskog, and M.Pettersson, ACS Nano **4**, 6781 (2011).

[26] F.Xia, M.Steiner, Y.-M.Lin, and Ph.Avouris, Nature Nanotechn. **6**, 609 (2008).

[27] A.Hoegele, Ch.Galland, M.Winger, and A.Imamoglu, Phys. Rev. Lett. **100**, 217401 (2008).

[28] I.V.Bondarev, J. Comp. Theor. Nanosci. **7**, 1673 (2010); J. Electron. Mater. **36**, 1579 (2007).

[29] C.D.Spataru and F.Léonard, Phys. Rev. Lett. **104**, 177402 (2010).

[30] Y.Zhang, T.-T.Tang, C.Girit, Z.Hao, M.C.Martin, A.Zettl, M.F.Crommie, Y. Ron Shen, and F.Wang, Nature **459**, 820 (2009).

[31] I.V.Bondarev Phys. Stat. Sol. B **248**, 468 (2011); Superlattices and Microstructures **49**, 217 (2011).

[32] Electrostatic fields reported for the QCSE on CNs must be multiplied by $1/\sqrt{4\pi\epsilon_0}$ to result in field strengths $\sim$V/nm, consistent with fields observed for the QCSE on bilayer graphene [30]. I.V.B. is indebted to Dr. A.Hoegele of LMU, Germany, for bringing this issue to his attention.

[33] D.J.Bergman and M.I.Stockman, Phys. Rev. Lett. **90**, 027402 (2003).

[34] R.P.Feynman, *Statistical Mechanics* (W.A.Benjamin, Inc., Massachusetts, 1972).

[35] Y.Murakami and J.Kono, Phys. Rev. Lett. **102**, 037401 (2009).

[36] V.Bagnato and D.Kleppner, Phys. Rev. A **44**, 7439 (1991); W.-S.Dai and M.Xie, Phys. Rev. A **67**, 027601 (2003).

[37] T.Ando, J. Phys. Soc. Jpn. **74**, 777 (2005).

[38] T.Pichler, M.Knupfer, M.S.Golden, J.Fink, A.Rinzler, and R.E.Smalley, Phys. Rev. Lett. **80**, 4729 (1998).

[39] L.D.Landau and E.M.Lifshitz, *Statistical Physics* (Pergamon, Oxford, 1980).

[40] J.Kasprzak, M.Richard, S.Kundermann, A.Baas, P.Jeambrun, J.M.J.Keeling, F.M.Marchetti, M.H.Szymanska, R.Andre, J.L.Staehli, V.Savona, P.B.Littlewood, B.Deveaud, and L.S.Dang, Nature **443**, 409 (2006).